Biochimica et Biophysica Acta 1788 (2009) 1116–1125

Contents lists available at ScienceDirect

Biochimica et Biophysica Acta

journal homepage: www.elsevier.com/locate/bbamem

Comparison of the membrane interaction mechanism of two antimicrobial RNases: RNase 3/ECP and RNase 7

Marc Torrent [a], Daniel Sánchez [a], Víctor Buzón [b], M. Victòria Nogués [a], Josep Cladera [b], Ester Boix [a,*]

[a] Departament de Bioquímica i Biologia Molecular, Facultat de Biociències, Universitat Autònoma de Barcelona, 08193 Cerdanyola del Vallès, Spain
[b] Dpt. Bioquímica i Biologia Molecular, Unitat de Biofísica, Fac. Medicina, Universitat Autònoma de Barcelona, 08193 Cerdanyola del Vallès, Spain

ARTICLE INFO

Article history:
Received 2 October 2008
Received in revised form 27 December 2008
Accepted 17 January 2009
Available online 2 February 2009

Keywords:
Antimicrobial protein
Membrane
Liposome
Confocal microscopy
Fluorescence spectroscopy
RNase

ABSTRACT

Eosinophil cationic protein (ECP/RNase 3) and the skin derived ribonuclease 7 (RNase 7) are members of the RNase A superfamily. RNase 3 is mainly expressed in eosinophils whereas RNase 7 is primarily secreted by keratinocytes. Both proteins present a broad-spectrum antimicrobial activity and their bactericidal mechanism is dependent on their membrane destabilizing capacities. Using phospholipid vesicles as membrane models, we have characterized the protein membrane association process. Confocal microscopy experiments using giant unilamellar vesicles illustrate the morphological changes of the liposome population. By labelling both lipid bilayers and proteins we have monitored the kinetic of the process. The differential protein ability to release the liposome aqueous content was evaluated together with the micellation and aggregation processes. A distinct morphology of the protein/lipid aggregates was visualized by transmission electron microscopy and the proteins overall secondary structure in a lipid microenvironment was assessed by FTIR. Interestingly, for both RNases the membrane interaction events take place in a different behaviour and timing: RNase 3 triggers first the vesicle aggregation, while RNase 7 induces leakage well before the aggregation step. Their distinct mechanism of action at the membrane level may reflect different *in vivo* antipathogen functions.

1. Introduction

Ribonucleases (RNases) are found in all living organisms and play an important role in the metabolism of cellular RNA. However, other biological functions rather than the intrinsic ribonucleolytic activity have been described for several members of the RNase A superfamily [1–3]. Several RNases have antipathogen activities [4–6] and an ancestral host defense function was suggested [7].

The eosinophil cationic protein (ECP or RNase 3) is a human host defense ribonuclease involved in inflammatory processes mediated by eosinophils. ECP is a potent cytotoxic molecule, has bactericidal and helminthotoxic properties and is active against the respiratory syncytial virus (RSV). The ECP levels in different biological fluids correlate with the eosinophil activity and are used as an inflammatory marker [8,9].

Lehrer et al. first reported ECP bactericidal action and the protein ability to permeabilize the outer and inner *E. coli* membranes [10]. ECP bactericidal activity is indeed effective against both Gram-negative and Gram-positive strains [10–12] and its antimicrobial activity is dependent on its action at the cytoplasmic membrane and bacteria wall levels [13,14]. Early studies by Young and collaborators [15] already reported ECP ability to destabilize synthetic lipid bilayers. ECP bactericidal activity correlates with its membrane disruption ability and is dependent upon both surface exposed hydrophobic and cationic residues [12,16]. ECP can bind and partially insert into the lipid bilayers, promoting the lipid vesicles aggregation and lysis, following a “carpet like” mechanism [13].

Ribonuclease 7 is an antimicrobial protein expressed in skin, liver, kidney, skeletal muscle and heart [17,18]. It shows a low RNase activity in degradation of yeast tRNAs and has no antiviral activity for the respiratory sincitial virus. Human RNase 7 was originally identified from a screening protocol searching for antimicrobial proteins in skin. RNase 7 revealed a broad spectrum antimicrobial activity against Gram-negative and Gram-positive strains [17,19], and a remarkably potent activity against *Enterococcus faecium* [17]. RNase 7 has also a high antimicrobial activity against *Pseudomonas aeruginosa* and the yeast *Pichia pastoris* [20]. RNase 7 mRNA expression was detected in various epithelial tissues including skin, gut, respiratory and genitourinary tract [19]. RNase 7 expression responds to inflammatory agents and bacterial infection [17]. Molecular cloning from skin-derived primary keratinocytes and purification of RNase 7 from supernatants of cultured primary cells indicate that keratinocytes represent the major cellular source in skin. In addition to a constitutive expression,

Abbreviations: DOPC, 1,2-Dioleoyl-*sn*-glycero-3-phosphocholine; DOPG, 1,2-dioleoyl-*sn*-glycero-3-[phospho-rac-(1-glycerol)]; ANTS, 8-Aminonaphthalene-1,3,6-trisulfonic acid disodium salt; DPX, *p*-xylene-bispyridiniumbromide; LUV, large unilamellar vesicles; GUV, giant unilamellar vesicles

* Corresponding author. Tel.: +34 93 5814147; fax: +34 93 5811264.
E-mail address: Ester.Boix@uab.es (E. Boix).

0005-2736/$ – see front matter © 2009 Elsevier B.V. All rights reserved.
doi:10.1016/j.bbamem.2009.01.013

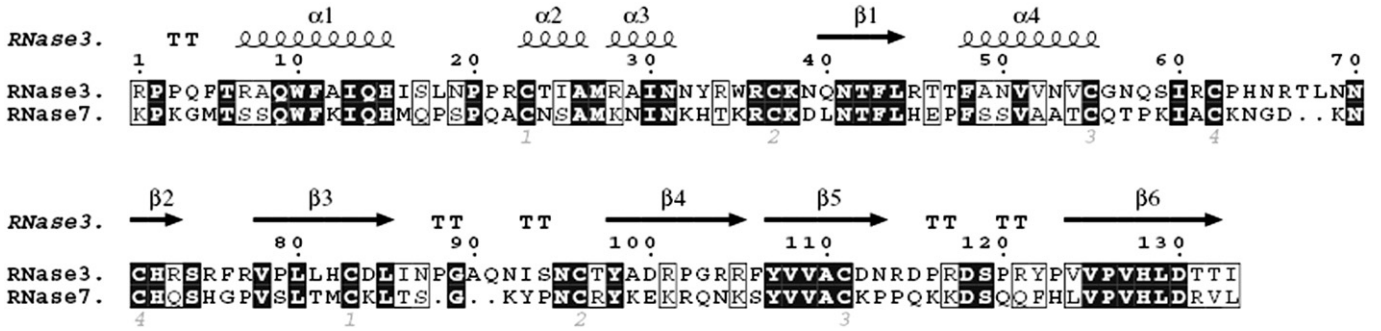

Fig. 1. Comparison of the blast alignment of RNase 3 and RNase 7 primary sequences. Secondary structure of RNase 3 is depicted. Strictly conserved residues are boxed in dark grey, and conserved residues, as calculated by a similarity score are boxed in white. Cysteine pairings for disulfide bridges are numbered below. The figure was created using the ESPrit software [48].

RNase 7 mRNA was induced in cultured primary keratinocytes by interleukin-1, interferon-, and bacterial challenge [17]. RNase 7 site-directed mutagenesis studies have identified some lysine clusters required for the protein antimicrobial action [20].

Both RNase 3 and RNase 7, as representative members of the RNase A family, display RNase activity for most common RNA substrates, although its RNase activity has been reported not necessary for the antibacterial action [11,20].

In this study we present a comparison of the interaction mechanisms of RNase 3 and RNase 7 with lipid bilayers using a synthetic membrane model. Although both proteins belong to the RNase superfamily and show a high cationicity, they have accumulated an unusual number of either Arg (RNase 3) or Lys (RNase 7) residues (Fig. 1) by a divergent evolution path. We present here evidences that both proteins exhibit a distinct membrane interaction behaviour.

2. Materials and methods

2.1. Materials

1,2-Dioleoyl-*sn*-glycero-3-phosphocholine(DOPC) and 1,2-dioleoyl-*sn*-glycero-3-[phospho-rac-(1-glycerol)] (DOPG) were from Avanti Polar Lipids, Birmingham, AL.

8-Aminonaphthalene-1,3,6-trisulfonic acid disodium salt (ANTS), *p*-xylene-bispyridiniumbromide (DPX), Alexa Fluor 488 Protein Labelling kit, Vibrant DiI cell-labelling solution and Concanavalin-Alexa Fluor 488 were from Molecular Probes, Invitrogen, Carlsbad, CA. pET11 expression vector and *E. coli* BL21(DE3) cells were from Novagen, Madison,WI. pFLAG CTS/RNase 7 was kindly provided by Helene Rosenberg (NIAID, NIH, Bethesda, Maryland).

2.2. Preparation of recombinant proteins

Construction of the RNase 7 expression plasmid was performed using the plasmid construct pFLAG CTS/RNase 7. Plasmid pFLAG CTS/RNase 7 [19] was subjected to polymerase chain reaction for subcloning of RNase 7 gene into the pET11c plasmid vector. The final sequence corresponds to RNase 7 lacking the leader sequence and having an additional N-terminal methionine residue (pET11c/RNase 7). RNase 3 was expressed using the previously constructed expression plasmid (pET11c/ECP) [21]. Protein expression in the *E. coli* BL21 (DE3) strain (Novagen, Madison, WI), folding of the proteins from inclusion bodies, and the purification steps were carried out as previously described [21].

2.3. LUV liposome preparation

Large unilamellar vesicles (LUVs) of a defined size (about 200 nm) were prepared as previously described (Torrent et al., 2007). LUVs were obtained from a vacuum-drying lipid chloroform solution by extrusion through 800, 400, and 200 nm polycarbonate membranes. The lipid suspension was frozen and thawed ten times prior to extrusion. Liposomes were obtained containing either DOPC/DOPG (3:2 molar ratio), or pure DOPC. A 1 mM stock solution of liposome suspension in 10 mM Tris–HCl and 0.1 M NaCl at pH 7.4 was prepared.

2.4. LUV liposome aggregation

Aggregation of LUV lipid vesicles was monitored by measuring the absorbance at 470 nm (A_{470}) using a Cary 400 spectrophotometer and cuvettes with an optical path of 1 cm. Prior to the addition of proteins, the vesicles were allowed to equilibrate for 15 min. Final assay conditions were: 200 μM lipid concentration and from 0.04 to 2 μM protein range concentration, in 10 mM HEPES, pH 7.4 buffer.

2.5. Dynamic light scattering

Changes in liposome population were analysed using a Microtrac Ultrafine Particle Analyser 150 spectrometer (UPA). This device measures vesicle size distribution by dynamic light scattering operating with heterodyne detection [22]. The UPA is equipped with a diode laser with a wavelength of 780 nm and a nominal output of 3 mW of optical power. RNases and DOPC/DOPG LUV were incubated at room temperature and the mean size of liposome population was recorded. The incubation buffer was 10 mM Tris–HCl, and 0.1 M NaCl, pH 7.4. Measurements were performed at 1.5 mM final liposome concentration and the protein concentration used was 1.5 μM and 3.75 μM to achieve a protein–lipid ratio of 1/1000 and 1/400 respectively. The results are presented as the volume (or weight) distribution.

2.6. GUV liposome preparation

Giant unilamellar vesicles (GUVs) were used for confocal microscopic observation of the membrane disruptive effects of the proteins. To obtain GUVs, we used the method of Needham et al. [23] with some modification. Briefly, DOPC:DOPG lipids (3:2) or pure DOPC were dissolved together in chloroform to a final concentration of 10 mg/mL. Subsequently, 200 μL aliquots were placed in the bottom of a 1.5-cm diameter, 10-mL glass tube. When required, phospholipids were labelled by adding 1 μl of Vibrant DiI solution and the sample was gently mixed with a vortex. The solvent was dried at room temperature in a stream of nitrogen gas, to provide a thin lipid film. After removal of residual solvent under high vacuum for at least 1 h, the film was prehydrated with a stream of water-saturated air for 30 min at 43–45 °C and then fully rehydrated by addition of 5 mL of a 0.1 M saccharose solution. The liposomes, which appear as an almost transparent, milky-pinked cloud in the middle of the solution, were collected and stored at 4 °C in polypropylene tubes. GUV liposome concentration was checked to be 1 mM final concentration. Vesicles obtained by this procedure had diameters ranging from 2 to 15 μm.

2.7. ANTS/DPX liposome leakage assay

The ANTS/DPX liposome leakage fluorescence assay was performed as described previously [13]. Briefly, a single population of LUV of DOPC:DOPG 3:2 composition containing 12.5 mM ANTS, 45 mM DPX, 20 mM NaCl, and 10 mM Tris–HCl at pH 7.5 was obtained. Unencapsulated material was separated from the vesicles by gel filtration on Sephadex G-25 (Amersham Pharmacia Biotech) using 20 mM Tris–HCl at pH 7.5 containing 0.1 M NaCl as an elution buffer. The lipid concentration was determined by a colorimetric assay method for free and phosphorylated glyceric acids [24]. The ANTS/DPX liposome suspension was diluted to a 30 μM final lipid concentration and was incubated at room temperature in the presence of the protein. The leakage activity was assayed at different protein concentrations (from 0.04 to 3 μM) by following the release of the liposome content. Fluorescence was measured using a 386 nm excitation wavelength and 535 nm emission wavelength. Slits were set at 5 and 10 nm for excitation and emission, respectively. Cut-off filters for excitation and emission wavelengths were set at 250–395 and 430–1100 nm, respectively. The percentage of leakage (% L) produced by the proteins after 1 h of incubation with the liposomes was calculated with the following equation: $\%L = 100 - \frac{F_p - F_0}{F_{100} - F_0}$, where F_p is the final fluorescence intensity after the addition of the protein (1 h), F_0 and F_{100} are the fluorescence intensities before the addition of the protein and after the addition of 0.5% Triton X-100. For each protein concentration, three calculated leakage values were averaged.

2.8. Fluorescent labelling of RNases

RNase 3, RNase 7 and RNase A were labelled with the *Alexa Fluor 488* fluorophor, following the manufacturer's instructions, as previously described [14]. To 0.5 mL of a 2 mg/mL protein solution in phosphate saline buffer (PBS), 50 μL of 1 M sodium bicarbonate, pH 8.3, were added. The protein is incubated for 1 h at room temperature, with the reactive dye, with stirring, following the manufacturer's conditions. The labelled protein was separated from the free dye by a PD10-desalting column.

2.9. Confocal microscopy

Experiments were carried out in a glass-coverslide system. 10 μl of 1 mM GUV liposomes were mixed with different concentrations of RNase 3 or RNase 7 (1–10 μM) and images were immediately recorded. RNase A was used in all cases as a negative control. Confocal images of the liposomes were captured using a laser scanning confocal microscope (Leica TCS SP2 AOBS equipped with a HCX PL APO 63 × 1.4 oil immersion objective, Germany). RNase 3 and RNase 7 labelled with Alexa Fluor 488 were excited using a 488-nm argon laser (515–540 nm emission collected) and Vibrant DiI was excited using an orange diode (588–715 nm emission collected). Similar experiments were carried out using Alexa Fluor 488-RNase A as a control. For time-lapse experiment, Life Data Mode software (Leica) was used, obtaining an image every 30 s in 30 min of total time experiment.

To probe high molecular weight compound leakage, liposomes containing concanavalin A-Alexa Fluor 488 (~104 kDa) were used. Concanavalin GUV liposomes were prepared as described above, using a 0.1 M saccharose, 10 mM concanavalin A-Alexa Fluor 488 rehydratation solution. Unencapsulated material was separated from the vesicles by gel filtration on Sephadex G-25 (Amersham Pharmacia Biotech) using 0.1 M saccharose solution as elution buffer. Profile analysis of fluorescence intensity was measured using the Leica Confocal Software.

2.10. Transmission electron microscopy

Transmission electron microscopy was applied to visualize the morphology of protein/lipid aggregates, following the described methodology [25] with minor modifications. Briefly, LUV liposomes were diluted at a final concentration of 200 μM, and incubated with 0.5 mM of RNase 3 or 1 mM of RNase 7 in 10 mM HEPES buffer, pH 7.4. The mixtures were incubated at room temperature for 40 min, after which 20 μL of samples were applied to carbon-coated grids and negatively stained with uranil acetate. Samples were examined in a JEOL JEM 2011 (Jeol Ltd., Tokio, Japan) transmission electron microscope.

2.11. Fourier transformed infrared spectroscopy (FTIR)

For the FTIR measurements, lyophilized RNase 3 or RNase 7 were dissolved in deuterated 10 mM buffer HEPES, pD 7.4. Protein samples were stored overnight in the corresponding deuterated buffer in order to ensure a complete H/D exchange. The samples were sandwiched between two CaF_2 windows separated by a 50-mm Teflon spacer at a final concentration of 10 mg/mL. LUV of DOPC:DOPG phospholipids were prepared to a final concentration of 10 mM. Protein–LUV samples were incubated for 15 min. The temperature was controlled with a Julabo circulating bath. For each spectrum, 1000 scans at a nominal resolution of 2 cm^{-1} were averaged with a sample shuttle device using a FTIR-Mattson Polaris spectrometer. The spectrometer was equipped with a cooled nitrogen mercury-cadmium-telluride (MCT) detector, and it was continuously purged with dry air (dew point lower than −60 °C). To obtain the pure spectrum of the protein, spectra of the solvent were recorded under identical conditions. The criterion for a good subtraction was to obtain a flat line between 1800 cm^{-1} and 2000 cm^{-1}. All spectra were also corrected for atmospheric water. The spectra were deconvoluted using an FHHH of 15 cm^{-1} and a k factor of 1.8. In order to measure the relative areas of the amide I9 band components, deconvoluted spectra were curve-fitted by means of a least-squares iterative program.

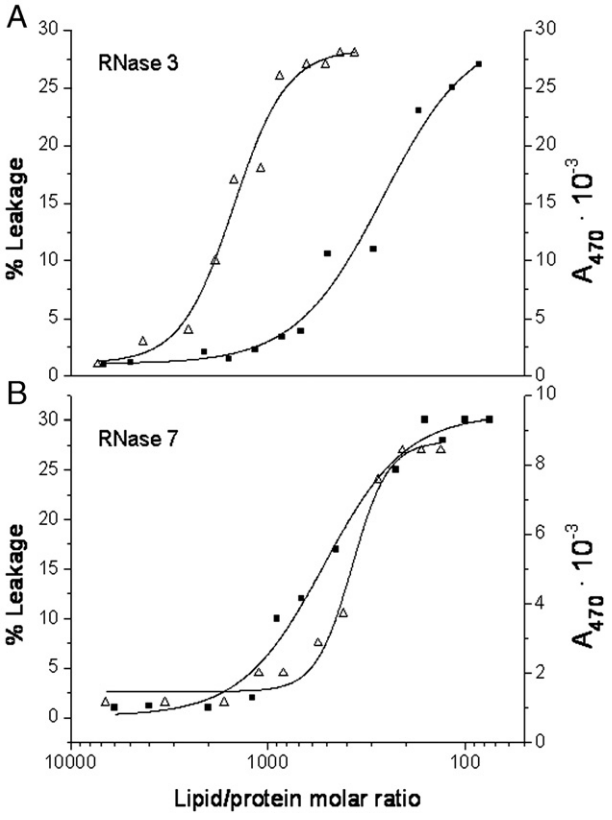

Fig. 2. Profile comparison of the aggregation and leakage processes as a function of the lipid/protein molar ratio, registered after 1 hour of incubation of the LUV with (A) RNase 3 and (B) RNase 7. Liposome aggregation was followed by recording the increase of absorbance at 470 nm and leakage activity was assayed by registering the release of the ANTS/DPX liposome content. Filled squares (leakage) and empty triangles (aggregation).

3. Results

3.1. LUV liposome aggregation

The increase of absorbance at 470 nm wavelength and DLS analysis were used to evaluate the lipid vesicle aggregation process after protein addition. DLS registered no increase in the mean size diameter of liposomes population for DOPC vesicles, even at a 1/100 protein/lipid molar ratio [13]. The lack of aggregation activity when using DOPC LUV was now also confirmed for both RNases. The spectrophotometric method was proven useful to monitor the liposome aggregation process (Fig. 2), corroborating the data recorded by dynamic light scattering [13].

RNase 3 begins to induce lipid vesicle aggregation at a protein/lipid molar ratio of 1/2000 and achieves a 50 % effect at a 1/900 protein/lipid molar relation. (Fig. 2A). The data reveal a high RNase 3 ability to aggregate lipid vesicles from a nanomolar protein concentration range, which corresponds to a protein /lipid molar ratio of about 1/2000.

In the other hand, RNase 7, presents a lower aggregation ability as we cannot observe lipid vesicle aggregation until a protein/lipid molar ratio of 1/500 is reached and the 50 % effect is achieved at an approximately 1/300 relation (Fig. 2B).

DLS allowed a direct estimation of the evolution of the liposome population mean size at two representative protein/molar lipid ratios (Fig. 3). The size distribution at distinct time intervals up to 1 hour for a 1/400 and a 1/1000 protein/lipid molar ratio for both RNases illustrates the process progress for each condition. Comparison of the distribution profiles indicates a pronounced shift towards higher diameter size values for RNase 3 in relation to RNase 7.

The sigmoidal shape of liposome aggregation as a function of the lipid/protein ratio for both, RNase 3 and RNase 7 (Fig. 2), suggests a cooperative mechanism. In this line, both RNases have to accumulate several molecules at the lipid surface to trigger the aggregation process. These results show that despite the overall high cationicity of both proteins, and their structural primary and tertiary homology (Fig. 1), the aggregation behaviour is distinct, indicating that aggregation of lipid vesicles in RNase 3 is an earlier event than in RNase 7 in the protein–membrane interaction process.

3.2. ANTS/DPX liposome leakage assay

We have evaluated the proteins ability to trigger the leakage of the liposome aqueous content by the ANTS/DPX fluorescence assay. ANTS is a low molecular weight marker (427 Da) that allows the detection of local membrane disruption.

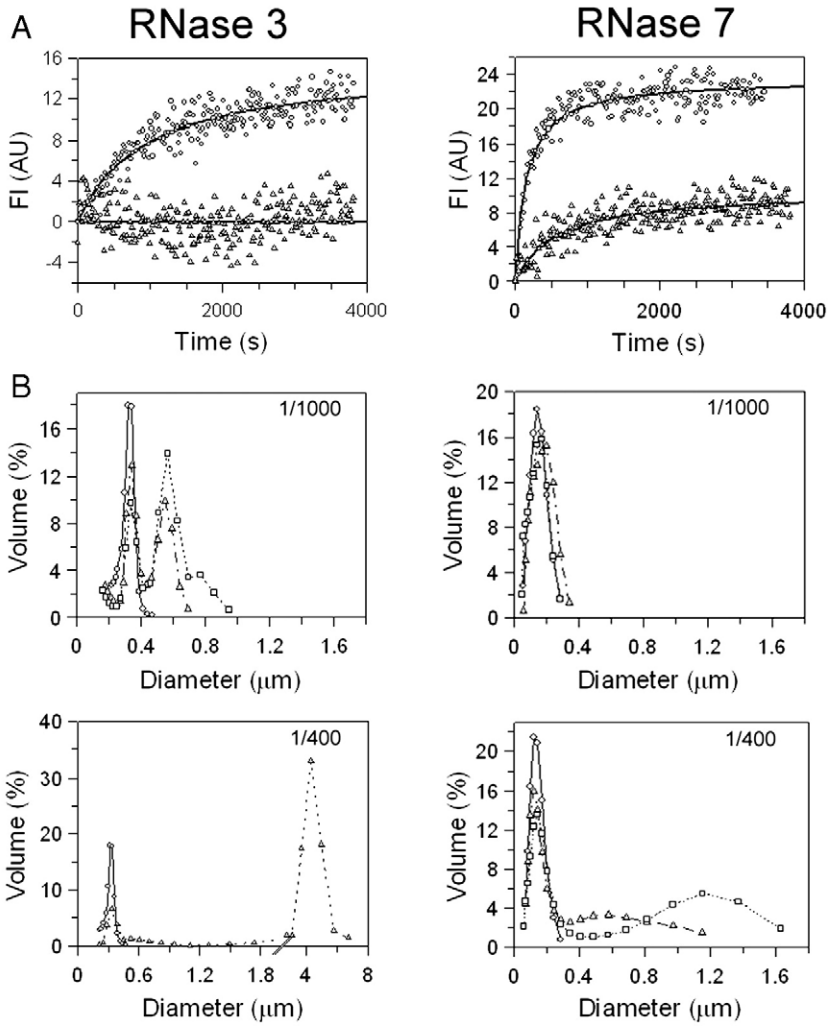

Fig. 3. Comparative kinetic analysis of the liposome aggregation and leakage processes triggered by RNases 3 and 7. (A) Leakage kinetics of 3:2 DOPC:DOPG liposomes incubated with RNase 3 and RNase 7 at 1/1000 (empty triangles) and 1/400 (empty circles) protein–lipid molar ratio. (B) Aggregation kinetics of 3:2 DOPC:DOPG liposomes incubated with RNase 3 and RNase 7 at 1/1000 and 1/400 protein–lipid molar ratio. Estimation of the average diameter size was assessed by DLS. Results are displayed as the volume percentage for each liposome diameter at different times: 0 min (empty circles), 20 min (empty triangles) and 60 min (empty squares). Incubation with RNase 3 for 60 min at 1/400 ratio lead to full sample precipitation and cannot be evaluated. Average diameter values over 2 μm cannot be accurately predicted and values are merely included in the graph for internal comparison.

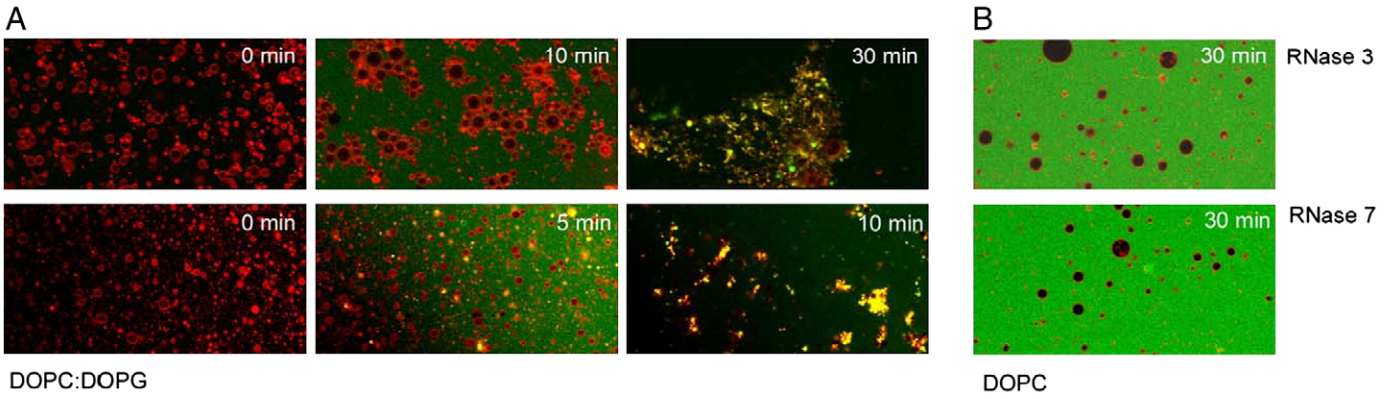

Fig. 4. Study of the liposome population morphology visualized by confocal microscopy. (A) DOPC/DOPG liposomes incubated with RNase 3 at 0, 10 and 30 min (top) and with RNase 7 at 0, 5 and 10 min (bottom). (B) DOPC liposomes after protein addition for 30 min. Proteins were labelled with AlexaFluor 488 (green signal) and liposomes with Vibrant DiI (red signal). Panels include the overlay of both signals. RNase 3 concentration was 4 μM (protein/lipid ratio 1/400) and RNase 7 concentration was 8 μM (protein/lipid ratio 1/200).

No leakage is detected when using pure DOPC LUV for both RNase 3 [12,13] and RNase 7 at even 1/30 protein/lipid ratio (data not shown). Using DOPC/DOPG LUV, leakage activity is registered as an increase in fluorescence intensity. No content release is detected when using RNase A as a control [12]. Both RNase 3 and RNase 7 show a significant leakage activity, although a distinct pattern is observed in each case (Fig. 2).

RNase 3 requires a higher protein concentration to present a significant leakage activity, which is registered at a protein/lipid ratio of 1/300 (Fig. 2A). This leakage ability is shown with a considerable delay after the onset of the liposome vesicle aggregation. These results suggest that RNase 3 leakage activity is induced by membrane destabilization when vesicle aggregation has already taken place. The

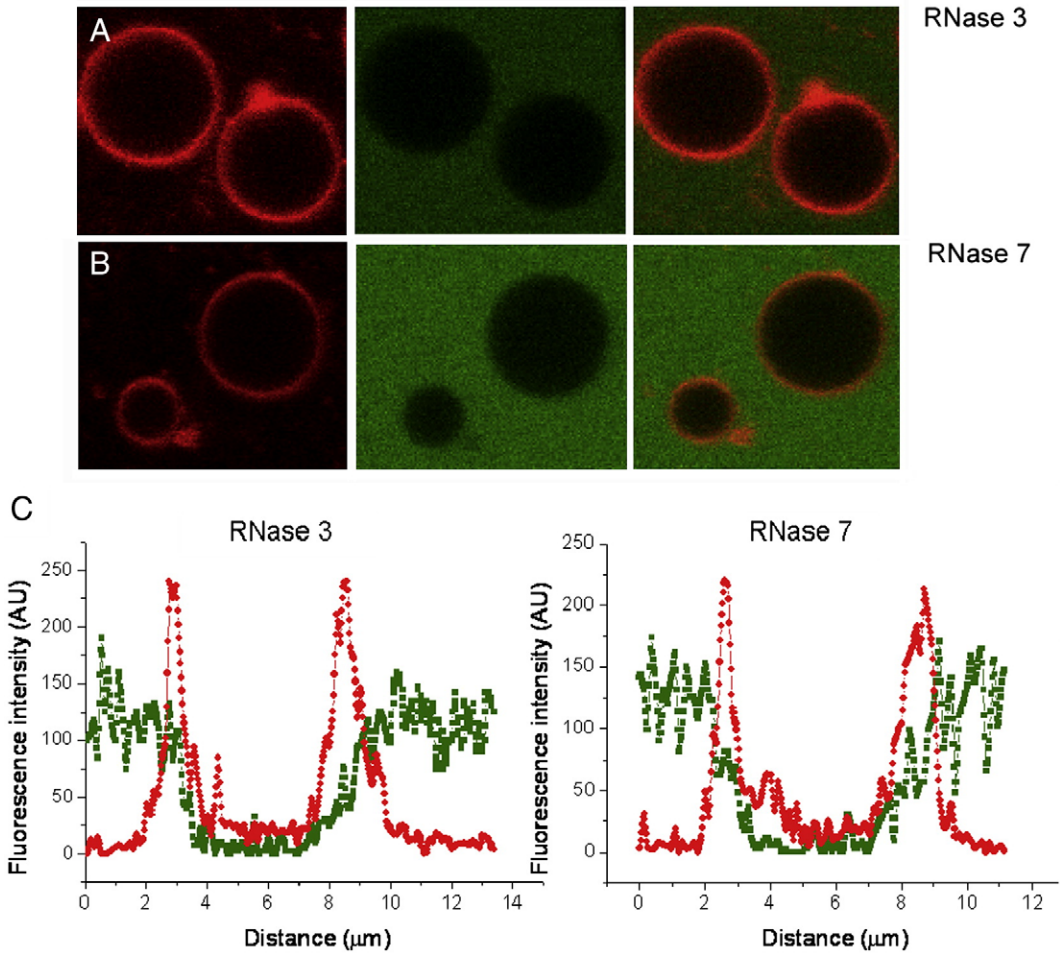

Fig. 5. Study by confocal microscopy of RNase 3 and RNase 7 location in the protein–lipid vesicles samples. Proteins were labelled with AlexaFluor 488 and phospholipids were labelled with Vibrant DiI. Left panels correspond to the Vibrant DiI fluorescent marker (red signal) excited using an orange diode (588–715 nm emission collected). Central panels correspond to the labelled proteins with Alexa Fluor 488 (green signal), excited using a 488-nm argon laser (515–540 nm emission collected). Right-hand panels correspond to the overlay of both signals. (A) RNase 3 incubation for 30 min with 3:2 DOPC/DOPG liposomes; (B) RNase 7 incubation for 30 min with 3:2 DOPC/DOPG liposomes and (C) profiles of fluorescence intensity for labelled RNases (in green) and phospholipids (in red). The graph represents a section of a single liposome. Protein concentration was 2 μM, corresponding to a protein/lipid molar ratio of 1/800.

release of the entrapped liposome content continues to increase parallel to the precipitation event (Fig. 2A), suggesting that the content release is a consequence of the aggregation process.

RNase 7, on its turn, presents a distinct behaviour. We observe that RNase 7 begins to present a leakage activity at a protein/lipid ratio above 1/900, corresponding to a much lower protein concentration. In fact RNase 7 can release the low molecular weight ANTS fluorofor before any aggregation event occurs (Fig. 2B).

A direct recording of the release of the liposome content indicates that the process is fast and the fluorescence signal reaches already a maximum plateau after 10–15 min (Fig. 3A). A side by side comparison of the kinetic of the aggregation and leakage processes during 1 hour confirms that RNase 3 triggers already the vesicles aggregation when no leakage is registered (protein/lipid ratio 1/1000). On the other hand, leakage is already detectable for RNase 7 at a 1/1000 ratio while no change on the liposome mean size is observed. Moreover, for RNase 7 at a 1/400 ratio, when a 20% of the liposome content is released, most of the vesicles still retain their original size.

3.3. Confocal microscopy

Confocal microscopy experiments using giant unilamellar vesicles (GUVs) allow the visualization of the conformational changes on the vesicle population triggered by protein incubation (Fig. 4). We have first confirmed that no activity is observed for pure neutral vesicles. The lack of activity on DOPC liposomes indicates again that the interaction process is electrostatically driven, as no leakage, fusion or aggregation is observed. The conformational changes of the DOPC/DOPG vesicle population have been monitored at different timing and protein concentrations. RNase 3 at 4 μM triggers rapidly the aggregation process, visible from 10 min onwards, and the lipid vesicles precipitation takes place after 30 min. In the initial aggregation stage, formation of protein–lipid patches in the membrane can be observed and an intensive vesiculation of liposomes is also remarkable (Fig. 4A).

The kinetic of the aggregation process for RNase 7 seems to be faster than RNase 3, but a minimum concentration of 10 μM has to be reached to observe it (Fig. 4A). Once this protein threshold is reached, the precipitation even takes place in only about 10 min. Moreover, although protein–lipid patches can also be observed, no prior aggregation has been detected in this case.

By labelling the proteins and liposomes with the specific fluorescent markers we could directly assess the membrane integrity and the protein behaviour, during the process of vesicle aggregation. We have confirmed that both RNases do not internalize into the liposome vesicles (Fig. 5). RNase 3 remains at the membrane level,

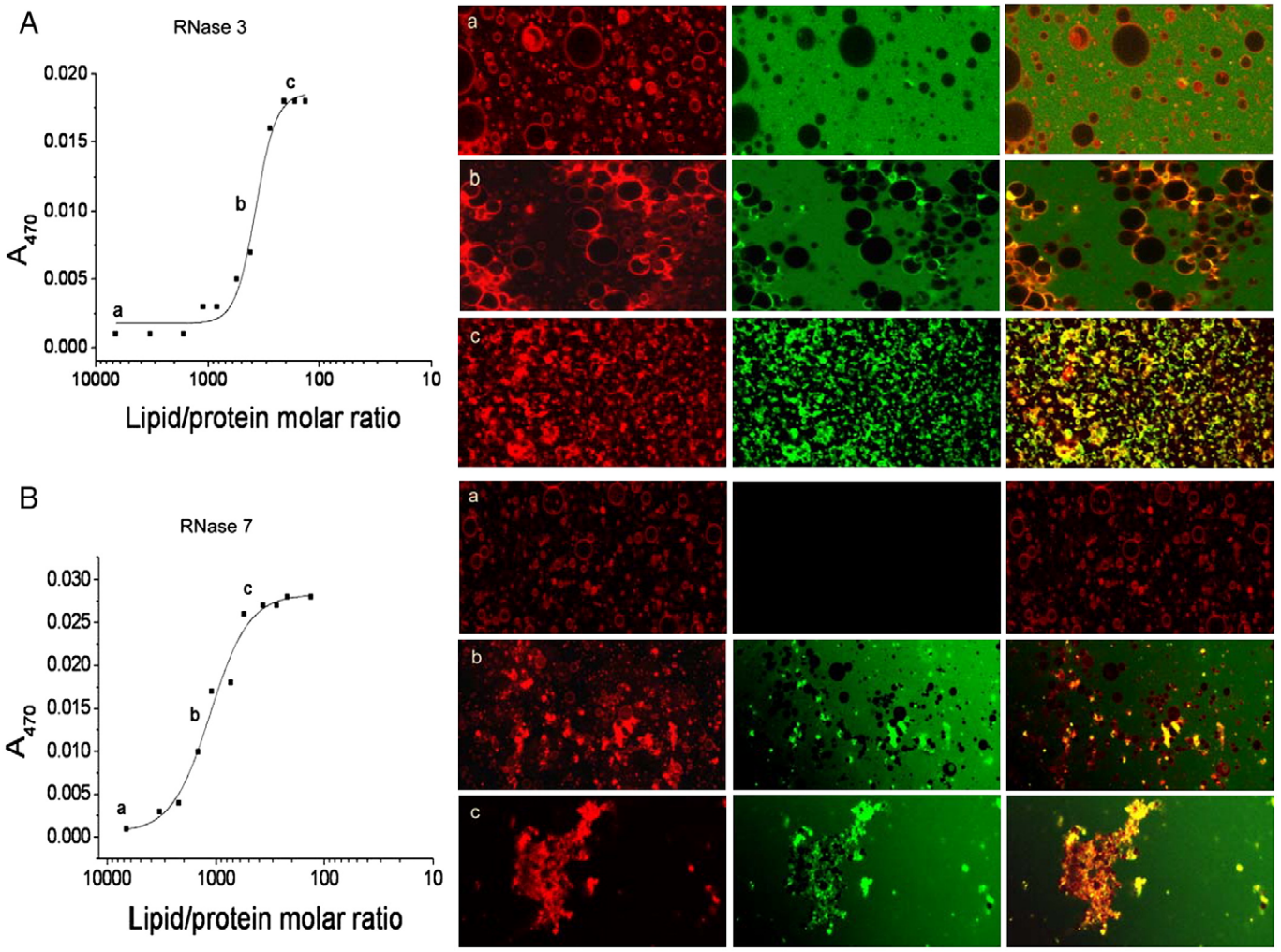

Fig. 6. Study on the liposome aggregation process by RNase 3 (A) and RNase 7 (B). Liposome aggregation process was followed by the visualization of liposome morphology by confocal microscopy upon incubation for 40 min. Proteins labelled with Alexa Fluor 488 (green signal) were excited using a 488-nm argon laser (515–540 nm emission collected) and Vibrant DiI (red signal) was excited using an orange diode (588–715 nm emission collected). Three representative protein/lipid molar ratio were chosen for the comparison of the distinct steps of the lipid vesicles aggregation process, taking as a reference the registered profile of the increase of the absorbance at 470 nm. A) RNase 3: a) 1 μM (lipid/protein ratio 1600); b) 2 μM (lipid/protein ratio 800) and c) 4 μM (lipid/protein ratio 400). B) RNase 7: a) absence of protein; b) 5 μM (lipid/protein ratio 200) and c) 10 μM (lipid/protein ratio 100).

first producing aggregation of lipid vesicles and then inducing its precipitation. In this line, labelled RNase 7 also remains at the membrane level and is not internalized into the vesicles. The fluorescence intensity profiles of a section of a single liposome also confirmed that no labelled proteins are internalized into the liposomes (Fig. 5C). We observe the Vibrant DiI red signal following the vesicle lipid bilayer and all the AlexaFluor green signal located at the external sides of the vesicle.

The liposome aggregation process analysed in detail by confocal microscopy, allows to distinguish three main steps (Fig. 6). For RNase 3 (Fig. 6A) we can identify a initial range (around a protein/lipid ratio of 1/2000) where the aggregation process is triggered but cannot be visualized by confocal microscopy (a). Aggregation is then patent at a value of 1/800 (b) and this aggregation may turn into vesicle–protein precipitation if the protein/lipid relation is increased at a value of 1/400 (c).

On its turn, RNase 7 (Fig. 6B) is able to induce aggregation of lipid vesicles from a protein/lipid ratio of 1/400 but this aggregation is not visible by confocal microscopy at a 1/200 ratio (b). This aggregation may turn into vesicle–protein precipitation if the protein/lipid relation is increased at a value of 1/100 (c). Confocal microscopy images suggest that both RNase produces vesicle aggregates with distinct morphological conformation, as further inspection by transmission electron microscopy corroborates.

Additionally, experiments with GUVs with incorporated concanavalin-Alexa Fluor 488 have also proven useful to directly assess any potential membrane disruption event. The results obtained using liposomes containing concanavalin A-Alexa Fluor 488 have shown that for RNase 7 there is no significant content release of high molecular weight compounds at protein/ lipid molar ratio where leakage of ANTS/DPX is already taking place (Fig. 7). The fluorescence intensity profiles of both concanavalin (green signal) and vesicle lipid bilayer (red signal) confirms that concanavalin is totally retained inside the vesicles (Fig. 7B).

The results suggest for RNase 7 a local membrane destabilization, forming protein–lipid structures that may release low molecular weight compounds whereas high molecular weight compounds remain encapsulated inside the liposome structure. However, confocal microscopy using liposomes containing concanavalin A-Alexa Fluor 488 could only be assessed by selecting isolated floating liposomes. Therefore, protein/lipid conditions where aggregation is predominant could not be analysed, and the methodology does not allow to check if the sedimented liposome aggregates retain or not the vesicles content.

In the case of RNase 3, the triggering of the leakage process requires higher protein concentrations, when aggregates are already formed, and therefore the concanavalin experiment was not feasible. Besides, the analysis would not provide any additional information, as RNase 3 would trigger the vesicles lysis, releasing simultaneously the low and high molecular weight markers.

3.4. Transmission electron microscopy

TEM micrographs of negatively stained samples allowed the visualization of the protein–lipid precipitate. This technique was suitable to analyse the morphology of the vesicles aggregates (Fig. 8). A distinct conformation for the liposome aggregates is observed for both proteins, corroborating the pattern tendency suggested by confocal microscopy analysis. For both proteins we have analysed a precipitate sample obtained after incubation with the protein for 40 min at a protein/lipid ratio of 1/400 for RNase 3 and 1/200 for RNase 7, which corresponds to a condition where the aggregation process is completed. Big aggregates are observed in both cases. However, TEM images suggest that the aggregate conformation is distinct. While the final LUV aggregate triggered by incubation with RNase 7 is more dense and elongated; spherical structures retaining the liposomes original conformation are still patent in the RNase 3 / liposomes precipitate. This difference may depend on the distinct first step registered for both proteins, as drawn in the scheme depicted to

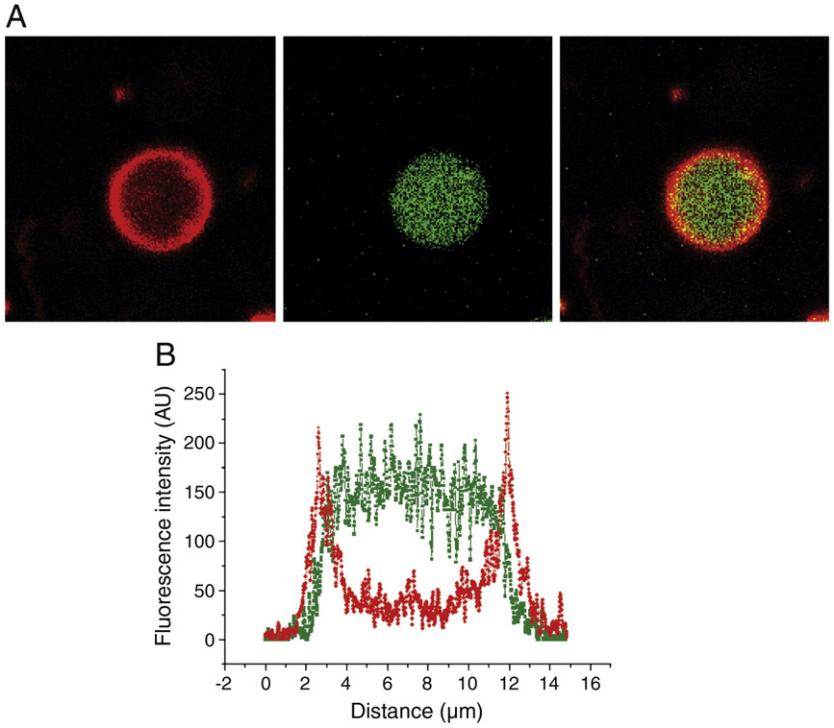

Fig. 7. (A) Confocal microscopy of concanavalin A containing liposomes incubated with RNase 7 for 30 min. Left panels correspond to the Vibrant fluorescent marker (red signal) excited using an orange diode (588–715 nm emission collected). Central panels correspond to the labelled concanavalin with Alexa Fluor 488 (green signal), excited using a 488-nm argon laser (515–540 nm emission collected). Right-hand panels correspond to the overlay of both signals. Images were taken at the protein/lipid molar ratio of 1/500, corresponding to a 50% of leakage activity. (B) Profiles of fluorescence intensity. AlexaFluor 488-concanavalin signal represented in green and Vibrant DiI labelled phospholipids signal in red. The graph represents a section of a single liposome.

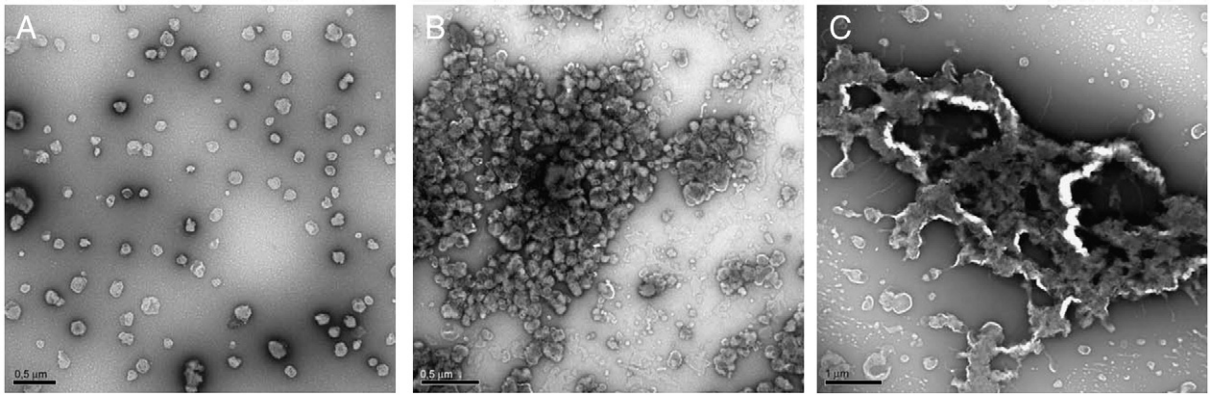

Fig. 8. TEM and negative staining micrographs of LUV incubated for 30 min at a 1/400 and 1/200 protein/lipid ratio for RNase 3 and RNase 7 respectively. Conditions were selected to visualize the final precipitate morphology: A) control, B) RNase 3 and C) RNase 7.

illustrate the proposed model (Fig. 9). While RNase 7 can induce the lysis of liposomes at a low protein concentration, before any vesicle aggregation is activated, RNase 3 is agglutinating "intact" vesicles. This would explain the formation for RNase 7 of more lipid supra structures, where the original LUV shape is completely lost.

3.5. Fourier transformed infrared spectroscopy (FTIR)

FTIR was used to monitor secondary structure changes during interaction of both, RNase 3 and RNase 7, with LUV liposome membranes. The deconvoluted spectra were obtained and peaks were identified according to the literature established assignments [26–28]. Previous FTIR spectra of RNase 3 at pD 5.5 and 7.5 were already characterized [29]. Using this technique, we have compared the overall protein structures in the absence and presence of lipid vesicles. No secondary structure modification of neither RNase 3 nor RNase 7 was detected. These results suggest that membrane lysis mechanism of action does not involve structure changes or modification of the protein overall conformation.

4. Discussion

RNase 3 and RNase 7 are human RNases potentially involved in host defense [3,4,20,30–34] that show a cytotoxic activity against a wide range of pathogens [5]. Their antimicrobial mechanism of action is mostly dependent on their membrane destabilization ability [4,8,20].

We have previously characterized RNase 3 bactericidal action [12,14] and its action on synthetic membrane models [12,13]. Analysis by electron microscopy and DLS revealed how the protein triggered

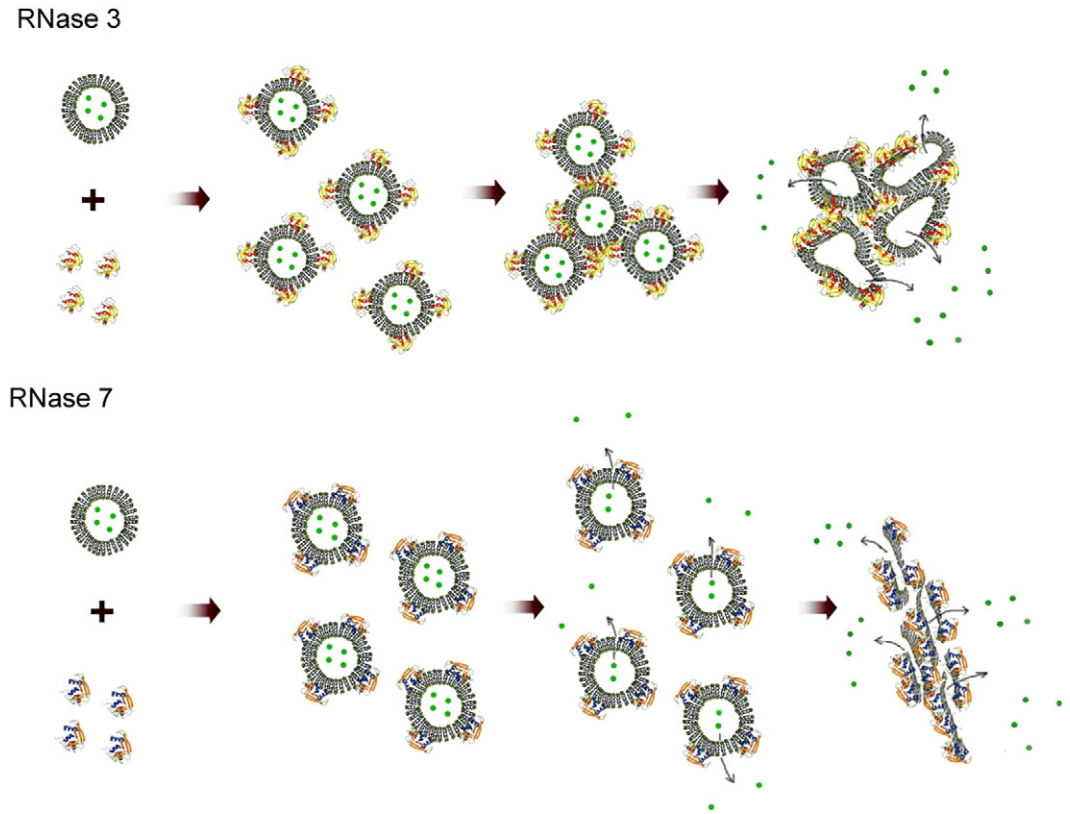

Fig. 9. Schematic drawing to illustrate the proposed timing of the events involved in the protein–lipid association process for RNases 3 and 7, as detailed in the discussion section. The proposed model includes the following steps: the protein molecules association to vesicles lipid bilayers, the vesicles aggregation process and the inner content release.

the lipid vesicle aggregation from a nanomolar concentration range, before any significant content leakage. A micellation process was also suggested and the results for RNase 3 were interpreted as indicative of a membrane destabilization "*carpet-like*" mechanism [13].

We have now further evaluated RNase 3 activity on synthetic membranes using LUV and GUV, and compared its action with RNase 7. Analysis of both RNases action by biophysical and microscopy methodologies, using as a model large and giant unilamellar lipid vesicles, allowed a careful characterization of the process.

We first confirmed that RNase 7 has neither aggregation nor vesicle leakage activity with pure neutral (DOPC) vesicles, as previously reported for RNase 3 [13]. Confocal microscopy results also revealed the lack of activity of both RNases on neutral liposomes (Fig. 4B). These results indicate that both, RNase 3 and RNase 7 mechanisms are electrostatically driven, as depletion of liposome charge practically abolishes protein–membrane interactions. As a result of the protein interaction with the phospholipid heads, the net charge of the environment would be reduced, and hydrophobic interactions would be promoted, and could perturb the phospholipid acyl chain core. These events would lead to the membrane destabilization and can explain the observed leakage of the entrapped low molecular weight markers and the micellation process visualized by confocal microscopy.

Although a first protein–lipid association step would be driven by electrostatic forces, leading to a final membrane disruption event for both RNases, further analysis of the interaction process reveals distinct mechanisms of action. We observe a differentiated timing and protein/lipid molar ratio required for the each of the membrane destabilization steps: vesicles content leakage, aggregation and sample precipitation (Figs. 2, 3, 4 and 6). RNase 3 triggers first the liposome aggregation while RNase 7 induces the liposomes content release before their aggregation (Fig. 3). In terms of protein/lipid molar ratio, whereas RNase 7 can induce leakage at a ratio of 1/900, RNase 3 requires a higher ratio (around 1/300) for a significant release of the liposome entrapped content (Fig. 2). On the other hand, whereas RNase 3 can trigger liposome aggregation at a very low protein/lipid ratio (<1/1000), RNase 7 needs a much higher ratio (1/400). These results indicate that vesicle aggregation is a key event for RNase 3 mechanism, whereas for RNase 7 the leakage event, rather than the vesicle aggregation ability, may represent the key triggering membrane destabilization step. Therefore, the comparative results indicate that for RNase 7, the first membrane destabilization step would represent only a local event, as the liposome content release is exclusive for the ANTS low molecular weight compound, whereas the high molecular weight tested compound concanavalin remains inside, even at much higher protein concentration (Fig. 7). Direct comparison of both leakage and liposome aggregation also confirms for RNase 7 that when a significant percentage of the leakage is already registered, the original vesicle population remains unaltered (Fig. 3). Besides, the lack of significant conformational change upon membrane interaction, as assessed by FTIR, also discards the formation of structured porus. We can propose that for both proteins, the membrane lysis would depend on the protein association to the lipid bilayer. The lack of activity for neutral vesicles indicates that association is driven by electrostatic interactions. Hydrophobic interactions might be involved then in the protein partial insertion and/or protein–protein binding. The accumulation of protein units at the membrane would finally induce its local destabilization.

Neither leakage nor aggregation ability was found for pancreatic ribonuclease A [12,13]. No membrane destabilization activity was either reported for the other eosinophil RNase, the eosinophil derived neurotoxin, EDN [15]. Protein aggregation prediction profile for the RNase A family members can support a differential sequence determinant for RNase 3 lipid vesicle aggregation ability [35]. A conserved pattern corresponding to the beta core of the protein, common to all ribonucleases is observed in all cases. On the contrary, more differences are observed at the N-terminus part. Whereas RNase 1, the human RNase A homolog, has a very low aggregation tendency in the N-terminus region, RNase 3 and RNase 7 present a higher aggregation propensity value. RNase 3 has indeed a hydrophobic patch at the N-terminus, with a higher propensity value spanning a more extensive region (from residues 8 to 18 and from 23 to 30). Scanning of RNase 7 shows only a narrower sequence corresponding to the first of the two N-terminus regions for RNase 3. These results may explain the higher capacity of RNase 3 to aggregate liposomes in comparison with RNase 7. We can propose that protein–protein interactions, favoured by association between hydrophobic patches, would mostly favour in RNase 3 the creation of an aggregation nucleus, which would trigger the liposomes precipitation process. The sigmoidal profile for the aggregation and leakage activities, as a function of the protein concentration (Fig. 2), suggests a dependence of the mechanism of action on the protein self aggregation from a threshold concentration value. In fact, we did visualize the presence of RNase 3 aggregated patches at the cell surface in the characterization of the cytotoxic process in eukaryote cell cultures [36].

We have also analysed the protein primary sequences to screen for potential significant differences for antimicrobial RNases (Fig. 1). Although, binding of cationic antimicrobial peptides to the cytoplasmic membrane does not appear to involve specific binding sites [37,38], some sequence determinants are reported for antimicrobial peptides. It is generally accepted that antimicrobial proteins and peptides need a combination of charged and hydrophobic amino acid residues [39–43]. Although ECP/RNase 3 and RNase 7 show only a 38% of sequence identity (Fig. 1), both share a high cationicity (with corresponding pI values of about 11 and 10 respectively), which should be critical for their antibacterial activity. However, careful inspection of their residue specificity indicates that their cationic character was acquired independently during the RNase A family evolution. While RNase 3 has incorpored a high number of arginine residues (18 Arg/1 Lys), during its divergence from the eosinophil RNases common precursor[44], RNase 7 presents an unusual high content of lysines (18 Lys/4 Arg), The positively charged/hydrophobic ratio has also been considered for comparison. RNase 3 presents a ratio of 19/42, while RNase 7 presents a lower ratio (22/51) (Fig. 1). These differences may also contribute to the observed distinct mechanisms for both ribonucleases. However, position and properties of hydrophobic residues should also be taken into consideration. The design of peptides with improved activity by high-throughput screening [45] indicates that some amino acid positions did not easily accept substitutions. A predictive methodology approach for the identification of active domains in antimicrobial proteins based on previous high-throughput screening results (Torrent et al., submitted) suggests a distinct pattern for RNase 3 and 7 potential active domains.

Fig. 9 tries to illustrate the proposed sequence of events involved in the protein–membrane association process, in an effort to interpret our experimental data accordingly to the described theoretical models from the literature [39,46,47]. Main steps of the proposed mechanism for each RNase could be summarized as follows. For RNase 3: 1) binding of the protein to the membrane phospholipid polar heads by electrostatic interactions; 2) clustering of the liposome–protein complexes; 3) liposome aggregation and destabilization of the lipid bilayer and 4) precipitate formation with the consequent membrane disruption and release of the liposome content. As for RNase 7, some of the events would occur in a distinct chronology: 1) binding of the protein to the membrane by electrostatic interactions; 2) local membrane destabilization allowing the formation of transient "holes"; 3) clustering of liposomes and 4) aggregation and final precipitate formation.

Interestingly, the expression pattern of these two RNases differs substantially. Whereas RNase 3 is mainly found in eosinophils, RNase 7 is expressed in multiple somatic tissues and predominantly in the

skin epithelial tissue. Their differential expression pattern and the current reported results on their action at the membrane level, suggest that these two RNases may be recruited for targeting different pathogens *in vivo*.

The pathogen selection may be reflected by a distinct cytotoxic mechanism, which is probably partly dependent on its membrane interaction mechanism, although other events that could take place at the bacterial wall level should also be considered. In fact, action at both the bacteria surface and cytoplasmic membrane do reveal a combined contribution ([14]; Torrent et al., unpublished results). Further characterization of RNases 3 and 7 properties will have to be carried to determine their pathogen target specificity and their biological functions.

Acknowledgements

Confocal microscopy and transmission electron microscopy were performed at the *Servei de Microscopia* of the Universitat Autònoma de Barcelona (UAB). We thank Mònica Roldán for her technical support. Spectrofluorescence assays were followed at the *Laboratori d'Anàlisi I Fotodocumentació*, UAB. We thank Helene F. Rosenberg at the NIAID, *National Institutes of Health*, for providing us a plasmid with RNase 7 cDNA. This work was supported by the *Ministerio de Educación y Cultura* (Grant BFU2006-15543-C02-01) and by the *Fundació La Marató de TV3* (TV3-031110). M.T. is the recipient of predoctoral fellowships from the *Generalitat de Catalunya*.

References

[1] J.Y. Dubois, B.M. Ursing, J.A. Kolkman, J.J. Beintema, Molecular evolution of mammalian ribonucleases 1, Mol. Phylogenet. Evol. 27 (2003) 453–463.
[2] E. Pizzo, G. D'Alessio, The success of the RNase scaffold in the advance of biosciences and in evolution, Gene 406 (2007) 8–12.
[3] K.D. Dyer, H.F. Rosenberg, The RNase a superfamily: generation of diversity and innate host defense, Mol. Divers 10 (2006) 585–597.
[4] H.F. Rosenberg, RNase A ribonucleases and host defense: an evolving story, J. Leukoc. Biol. 83 (2008) 1079–1087.
[5] E. Boix, M.V. Nogues, Mammalian antimicrobial proteins and peptides: overview on the RNase A superfamily members involved in innate host defence, Mol. Biosyst. 3 (2007) 317–335.
[6] E. Pizzo, M. Varcamonti, A. Di Maro, A. Zanfardino, C. Giancola, G. D'Alessio, Ribonucleases with angiogenic and bactericidal activities from the Atlantic salmon, FEBS J. 275 (2008) 1283–1295.
[7] S. Cho, J.J. Beintema, J. Zhang, The ribonuclease A superfamily of mammals and birds: identifying new members and tracing evolutionary histories, Genomics 85 (2005) 208–220.
[8] E. Boix, M. Torrent, D. Sánchez, M.V. Nogués, The antipathogen activities of eosinophil cationic protein, Curr. Pharm. Biotec. 9 (2008) 141–152.
[9] P. Venge, J. Bystrom, M. Carlson, L. Hakansson, M. Karawacjzyk, C. Peterson, L. Seveus, A. Trulson, Eosinophil cationic protein (ECP): molecular and biological properties and the use of ECP as a marker of eosinophil activation in disease, Clin. Exp. Allergy 29 (1999) 1172–1186.
[10] R.I. Lehrer, D. Szklarek, A. Barton, T. Ganz, K.J. Hamann, G.J. Gleich, Antibacterial properties of eosinophil major basic protein and eosinophil cationic protein, J. Immunol. 142 (1989) 4428–4434.
[11] H.F. Rosenberg, Recombinant human eosinophil cationic protein. Ribonuclease activity is not essential for cytotoxicity, J. Biol. Chem. 270 (1995) 7876–7881.
[12] E. Carreras, E. Boix, H.F. Rosenberg, C.M. Cuchillo, M.V. Nogues, Both aromatic and cationic residues contribute to the membrane-lytic and bactericidal activity of eosinophil cationic protein, Biochemistry 42 (2003) 6636–6644.
[13] M. Torrent, E. Cuyas, E. Carreras, S. Navarro, O. Lopez, A. de la Maza, M.V. Nogues, Y.K. Reshetnyak, E. Boix, Topography studies on the membrane interaction mechanism of the eosinophil cationic protein, Biochemistry 46 (2007) 720–733.
[14] M. Torrent, S. Navarro, M. Moussaoui, M.V. Nogues, E. Boix, Eosinophil cationic protein high-affinity binding to bacteria-wall lipopolysaccharides and peptidoglycans, Biochemistry 47 (2008) 3544–3555.
[15] J.D. Young, C.G. Peterson, P. Venge, Z.A. Cohn, Mechanism of membrane damage mediated by human eosinophil cationic protein, Nature 321 (1986) 613–616.
[16] E. Carreras, E. Boix, S. Navarro, H.F. Rosenberg, C.M. Cuchillo, M.V. Nogues, Surface-exposed amino acids of eosinophil cationic protein play a critical role in the inhibition of mammalian cell proliferation, Mol. Cell. Biochem. 272 (2005) 1–7.
[17] J. Harder, J.M. Schroder, RNase 7, a novel innate immune defense antimicrobial protein of healthy human skin, J. Biol. Chem. 277 (2002) 46779–46784.
[18] J.M. Schroder, J. Harder, Antimicrobial skin peptides and proteins, Cell. Mol. Life Sci. 63 (2006) 469–486.
[19] J. Zhang, K.D. Dyer, H.F. Rosenberg, Human RNase 7: a new cationic ribonuclease of the RNase A superfamily, Nucleic Acids Res. 31 (2003) 602–607.
[20] Y.C. Huang, Y.M. Lin, T.W. Chang, S.J. Wu, Y.S. Lee, M.D. Chang, C. Chen, S.H. Wu, Y.D. Liao, The flexible and clustered lysine residues of human ribonuclease 7 are critical for membrane permeability and antimicrobial activity, J. Biol. Chem. 282 (2007) 4626–4633.
[21] E. Boix, Z. Nikolovski, G.P. Moiseyev, H.F. Rosenberg, C.M. Cuchillo, M.V. Nogues, Kinetic and product distribution analysis of human eosinophil cationic protein indicates a subsite arrangement that favors exonuclease-type activity, J. Biol. Chem. 274 (1999) 15605–15614.
[22] O. Ostrowsky, Liposome size measurements by photon correlation spectroscopy, Chem. Phys. Lipids 64 (1993) 45–56.
[23] D. Needham, E. Evans, Structure and mechanical properties of giant lipid (DMPC) vesicle bilayers from 20 degrees C below to 10 degrees C above the liquid crystal–crystalline phase transition at 24 degrees C, Biochemistry 27 (1988) 8261–8269.
[24] G.R. Bartlett, Colorimetric assay methods for free and phosphorylated glyceric acids, J. Biol. Chem. 234 (1959) 469–471.
[25] A. de la Maza, J.L. Parra, O. Lopez, F. Congregado, N. Bozal, J. Guinea, Assembly properties of a glycoprotein produced by *Pseudoalteromonas antarctica*, NF3, J. Colloid Interface Sci. 192 (1997) 286–293.
[26] J. Cladera, M. Sabes, E. Padros, Fourier transform infrared analysis of bacteriorhodopsin secondary structure, Biochemistry 31 (1992) 12363–12368.
[27] D.M. Byler, H. Susi, Examination of the secondary structure of proteins by deconvolved FTIR spectra, Biopolymers 25 (1986) 469–487.
[28] E. Goormaghtigh, V. Cabiaux, J.M. Ruysschaert, Determination of soluble and membrane protein structure by Fourier transform infrared spectroscopy. II. Experimental aspects, side chain structure, and H/D exchange, Subcell. Biochem. 23 (1994) 363–403.
[29] Z. Nikolovski, V. Buzon, M. Ribo, M. Moussaoui, M. Vilanova, C.M. Cuchillo, J. Cladera, M.V. Nogues, Thermal unfolding of eosinophil cationic protein/ribonuclease 3: a nonreversible process, Protein Sci. 15 (2006) 2816–2827.
[30] L.V. Hooper, T.S. Stappenbeck, C.V. Hong, J.I. Gordon, Angiogenins: a new class of microbicidal proteins involved in innate immunity, Nat. Immunol. 4 (2003) 269–273.
[31] T. Nitto, K.D. Dyer, M. Czapiga, H.F. Rosenberg, Evolution and function of leukocyte RNase A ribonucleases of the avian species, *Gallus gallus*, J. Biol. Chem. 281 (2006) 25622–25634.
[32] B. Rudolph, R. Podschun, H. Sahly, S. Schubert, J.M. Schroder, J. Harder, Identification of RNase 8 as a novel human antimicrobial protein, Antimicrob. Agents Chemother. 50 (2006) 3194–3196.
[33] D. Yang, Q. Chen, S.B. Su, P. Zhang, K. Kurosaka, R.R. Caspi, S.M. Michalek, H.F. Rosenberg, N. Zhang, J.J. Oppenheim, Eosinophil-derived neurotoxin acts as an alarmin to activate the TLR2-MyD88 signal pathway in dendritic cells and enhances Th2 immune responses, J. Exp. Med. 205 (2008) 79–90.
[34] D. Yang, H.F. Rosenberg, Q. Chen, K.D. Dyer, K. Kurosaka, J.J. Oppenheim, Eosinophil-derived neurotoxin (EDN), an antimicrobial protein with chemotactic activities for dendritic cells, Blood 102 (2003) 3396–3403.
[35] O. Conchillo-Sole, N.S. de Groot, F.X. Aviles, J. Vendrell, X. Daura, S. Ventura, AGGRESCAN: a server for the prediction and evaluation of "hot spots" of aggregation in polypeptides, BMC Bioinformatics 8 (2007) 65.
[36] S. Navarro, J. Aleu, M. Jimenez, E. Boix, C.M. Cuchillo, M.V. Nogues, The cytotoxicity of eosinophil cationic protein/ribonuclease 3 on eukaryotic cell lines takes place through its aggregation on the cell membrane, Cell. Mol. Life Sci. 65 (2008) 324–337.
[37] Y. Chen, A.I. Vasil, L. Rehaume, C.T. Mant, J.L. Burns, M.L. Vasil, R.E. Hancock, R.S. Hodges, Comparison of biophysical and biologic properties of alpha-helical enantiomeric antimicrobial peptides, Chem. Biol. Drug Des. 67 (2006) 162–173.
[38] K. Hamamoto, Y. Kida, Y. Zhang, T. Shimizu, K. Kuwano, Antimicrobial activity and stability to proteolysis of small linear cationic peptides with D-amino acid substitutions, Microbiol. Immunol. 46 (2002) 741–749.
[39] M. Zasloff, Antimicrobial peptides of multicellular organisms, Nature 415 (2002) 389–395.
[40] J.P. Powers, R.E. Hancock, The relationship between peptide structure and antibacterial activity, Peptides 24 (2003) 1681–1691.
[41] K.L. Brown, R.E. Hancock, Cationic host defense (antimicrobial) peptides, Curr. Opin. Immunol. 18 (2006) 24–30.
[42] D. Andreu, L. Rivas, Animal antimicrobial peptides: an overview, Biopolymers 47 (1998) 415–433.
[43] K. Hilpert, M.R. Elliott, R. Volkmer-Engert, P. Henklein, O. Donini, Q. Zhou, D.F. Winkler, R.E. Hancock, Sequence requirements and an optimization strategy for short antimicrobial peptides, Chem. Biol. 13 (2006) 1101–1107.
[44] J. Zhang, H.F. Rosenberg, M. Nei, Positive Darwinian selection after gene duplication in primate ribonuclease genes, Proc. Natl. Acad. Sci. U. S. A. 95 (1998) 3708–3713.
[45] K. Hilpert, R. Volkmer-Engert, T. Walter, R.E. Hancock, High-throughput generation of small antibacterial peptides with improved activity, Nat. Biotechnol. 23 (2005) 1008–1012.
[46] Y. Shai, Mechanism of the binding, insertion and destabilization of phospholipid bilayer membranes by alpha-helical antimicrobial and cell non-selective membrane-lytic peptides, Biochim. Biophys. Acta 1462 (1999) 55–70.
[47] K. Matsuzaki, Why and how are peptide–lipid interactions utilized for self-defense? Magainins and tachyplesins as archetypes, Biochim. Biophys. Acta 1462 (1999) 1–10.
[48] P. Gouet, E. Courcelle, D.I. Stuart, F. Metoz, ESPript: analysis of multiple sequence alignments in PostScript, Bioinformatics 15 (1999) 305–308.